Jet Propulsion Laboratory
California Institute of Technology

Memorandum

AIRS ADF#620

To	AIRS Calibration Team	**From**	Margie Weiler
Department	JPL	Department	JPL/Swales Aerospace
Location		Location	P.O. Box 767, Bradford, NH 03221
Date	January 8, 2003	cc	
Telephone	[redacted]	Ref	
Fax	[redacted]		
Email	[redacted]		
Subject	Investigation of AIRS Correlated Noise		

I. SUMMARY

In a recent memo, Tom Pagano showed that, in many of the AIRS infrared detector modules, the noise exhibits substantial correlation from channel to channel.[1] This memo describes further investigations into the details of this correlation, using the same methodology. The following properties are shown:

1. The noise is correlated within each read-out integrated circuit (ROIC) module, not between modules.
2. The correlated noise is similar in all instrument environments.
3. The correlated noise is independent of the scene temperature.
4. Some modules have shown significant changes in the correlated noise with thermal cycles of the Focal Plane Array (FPA).
5. The temporal frequency spectrum of the correlated noise is approximately flat, i.e. it is not 1/f noise.
6. The strongest correlation is among channels with either A or B weights, and the correlation is weakest or even negative between channels with A and B weights.
7. The correlation of noisy channels shows a very broad distribution of values compared to low-noise channels.

A noise covariance matrix has been calculated from the C7/8 Space View Noise test data associated with each in-flight gain table.[2,3] These matrices are available for use in adjusting the weights in regression calculations using AIRS measured radiances.[4]

II. OVERVIEW OF ANALYSIS AND RESULTS

The noise characteristics of the AIRS infrared channels are estimated from the Space View Noise (C7/8) tests, in which the scan mirror is stopped for approximately 20 minutes, staring either at space or at the On-Board Calibrator (OBC). No DC restores are made during this time. These tests have been conducted in flight before and after each new A/B opt gain table upload (before, with A and B weights, after, with the new A/B Opt weights), and also were conducted as part of the thermal vacuum (T/Vac) tests at TRW and at BAE SYSTEMS (the latter with A and B weights only).

The data to be analyzed consist of approximately 440 scans of 90-footprint "scene" data and 4-footprint "space look" data, all viewing the same constant scene (space or OBC). These data are archived as *.mat* files in the *scene_data* and *cal_data* directories in either */scratch/act/mat_files* or *netapp1/insttest/sts/L1A2mat_files*. An analysis script *sv_nse_corr.m*, in */home/mweiler/C7_corr*, was written to retrieve these data files, call the STS script *get_signals.m* to perform the L1B/L2 standard median of 8 "space look" correction (*reference = 11*), and then calculate and plot the covariance matrix for all 2378 infrared detectors from the approximately 440x90 = 39,600 data points. As in Ref. 1, the Matlab *cov* function was used to calculate the covariance matrix

$$Cov(i,j) = \frac{1}{N}\sum_{k=1}^{N}\{R(k,i) - mean[R(i)]\}\{R(k,j) - mean[R(j)]\}$$

where *R(k,i)* is the data point for footprint *k* for channel *i*. The matrix is calculated in units of dn^2. The square root of each diagonal term gives the standard deviation for each channel.

Figure 1 shows an image plot for a typical *Cov(i,j)*. The blocks of correlated noise correspond, in order down the diagonal, to the 13 distinct photovoltaic (PV) ROIC modules in the AIRS FPA (M1a, M1b, M2a, M2b, M3, M4ab, M4cd, M5, M6, M7, M8, M9, M10), and to the 3 separate "clips" within the 2 photoconductive (PC) modules M11, and M12. The independent PV detector modules M4a and M4b share a single ROIC, here denoted M4ab; similarly M4c and M4d share the ROIC denoted M4cd. This establishes the important point that the correlated noise arises within each PV ROIC module or PC clip.

Figure 2 shows that similar patterns of correlated noise occurred in the T/Vac tests, both at BAE SYTEMS (instrument only) and at TRW (after spacecraft integration). Thus the correlated noise has occurred in all instrument environments. An important point to note is that this correlated noise cannot be cross-talk. Spectral test data showed no leakage of signal among channels; such a "pedestal" was found in the Engineering Model PC module and was eliminated in the Proto-Flight Model by implementing improved ground connections.

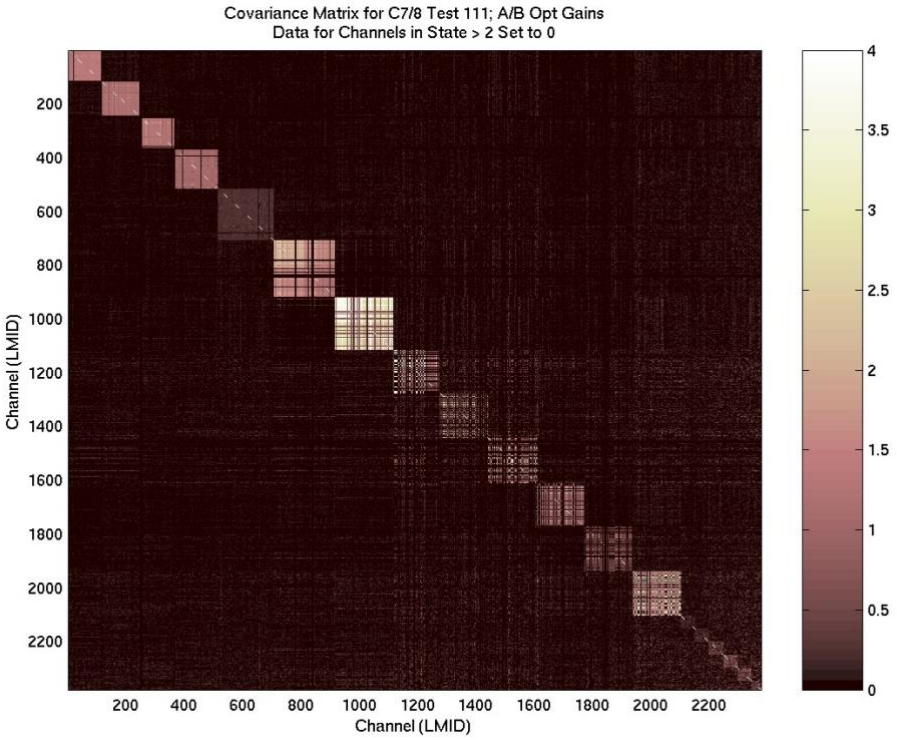

Figure 1. Image plot of the covariance matrix for in-flight C7 Space View Noise Test 111, with A/B Opt gains, showing blocks of within-module correlated noise.

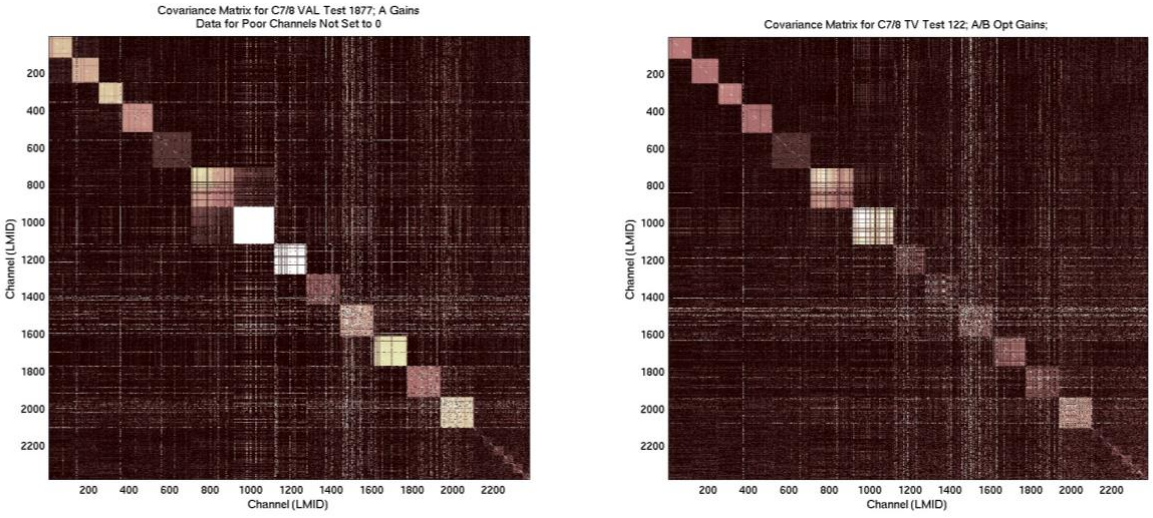

Figure 2. Image plots of the covariance matrices for two T/Vac C7 Space View Noise Tests: VAL 1877 (BAE STSTEMS, A gains) and TV 122 (TRW, A/B Opt gains).

III. SUMMARY OF STATISTICS BY MODULE

Inspection of Figures 1 and 2 shows that details of the covariance matrix have changed between these tests, reminiscent of the known changes in detector noise with FPA thermal cycles.[3] An approximate characterization of the covariance is to use the median of the diagonal and off-diagonal terms with each module.[1] The results for two tests are summarized in Table 1.

Table 1. Summary by module of the median diagonal and off-diagonal elements of the covariance matrix for C7/8 Tests 111 (viewing space) and 113 (viewing the OBC), and an estimate of the correlation coefficient for each module.

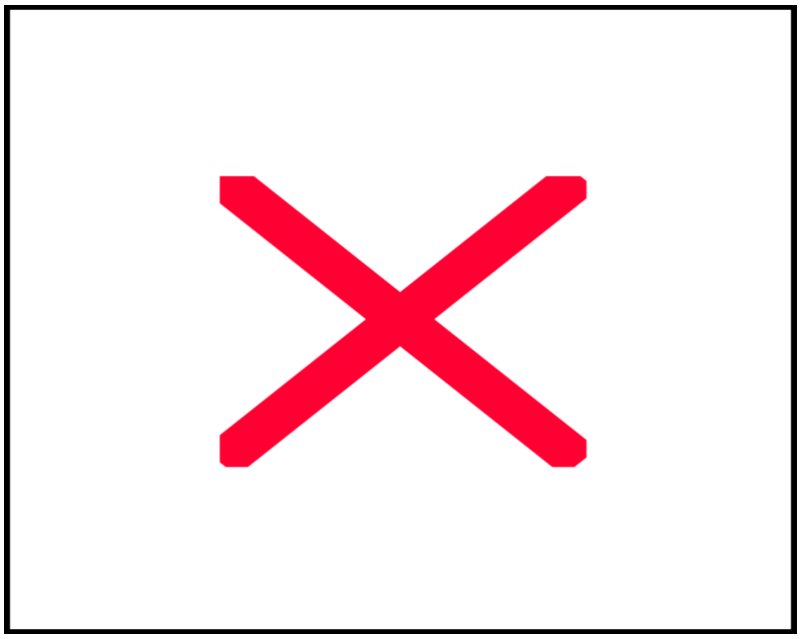

The results in Table 1 establish another important point, that the correlated (off-diagonal) noise is independent of the scene radiance, whereas, for some modules, there is a significant increase in the diagonal element with scene temperature. The table also includes an estimate of the correlation coefficient, defined as

$$corr\_coef(i,j) = Cov(i,j) / \sqrt{Cov(i,i)Cov(j,j)}$$

In Table 1 this is estimated as the ratio of the median off-diagonal term to the median diagonal term. The result can be used to estimate the significance of the correlation within each module (see also the plots in Ref. 1). The correlation is negligible for the PC modules M11 and M12, also quite small for the PV modules M3, M5, M6, M7, M9, and M10, and large for the PV modules M1, M2, M4, and M8.

For comparison, finite-size effects were estimated by calculating a covariance matrix for a 39,600 x 2378 array of random numbers resulting in maximum correlation coefficients of +/-0.026.

The test-to-test variability of the covariance matrix can be estimated by comparing the median values for the tests associated with the 5 in-flight gain tables, as shown in Table 2. In many cases there are small but still significant changes in both the diagonal and off-diagonal data. There is one exception, for Module 4c in Test 94, where changes in the population of two different covariance levels resulted in a large change in the median value. This is illustrated in Figure 3. Inspection of the A/B Opt gain tables for this module for these two tests shows no significant changes in the assigned states.[2]

Table 2. Summary by module of the median diagonal and off-diagonal elements of the covariance matrices for C7/8 Tests 21, 31, 55, 94. and 111 (viewing space, A/B Opt gains).

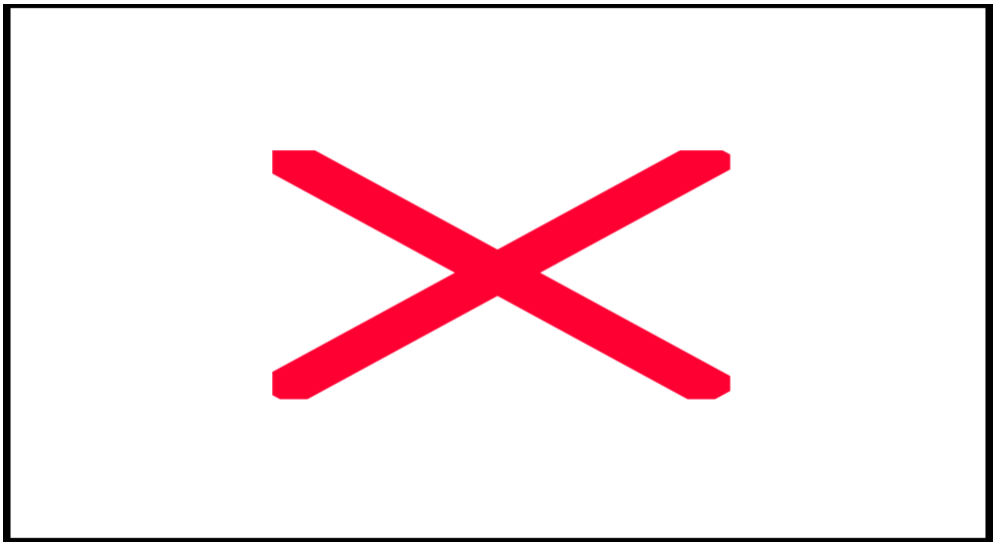

IV. TEMPORAL FREQUENCY DEPENDENCE

A test was made for 1/f behavior of the correlated noise by inspecting in detail the data for one of the more uniform modules, M1a. The data points for all "good" channels (in A/B Opt states 0-2) were summed, then an FFT was performed. The result, in Figure 4, shows very little low-frequency noise. The effective frequency is only approximate since these data consisted of 90 samples every 119 footprints; the analysis assumed uniform sampling of 90 footprints per scan cycle.

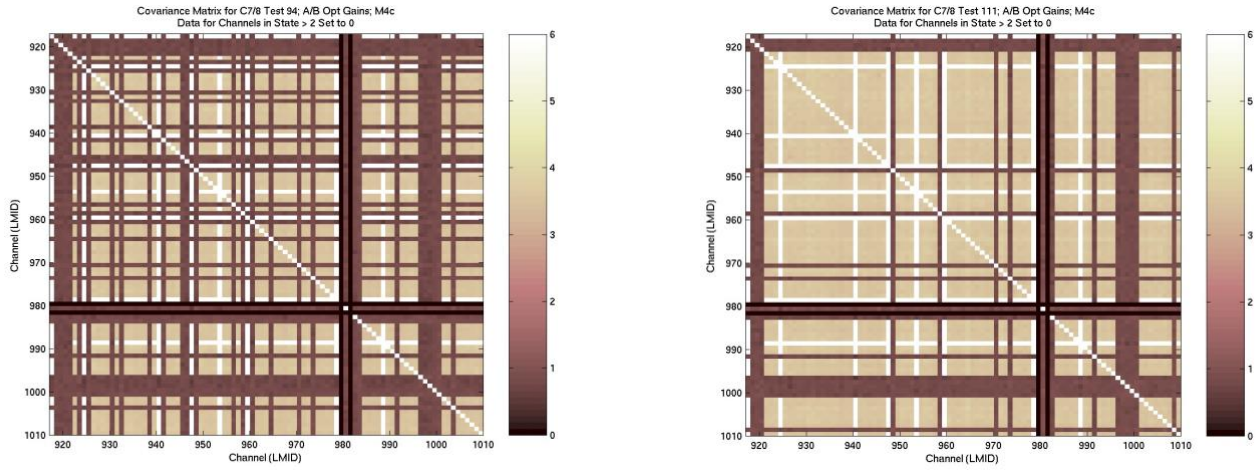

Figure 3. Image plots of the covariance matrix for Module M4c for two in-flight C7 Space View Noise tests from different FPA thermal cycles: Test 94 (left) and Test 111 (right) showing changes in the population of two different correlation levels.

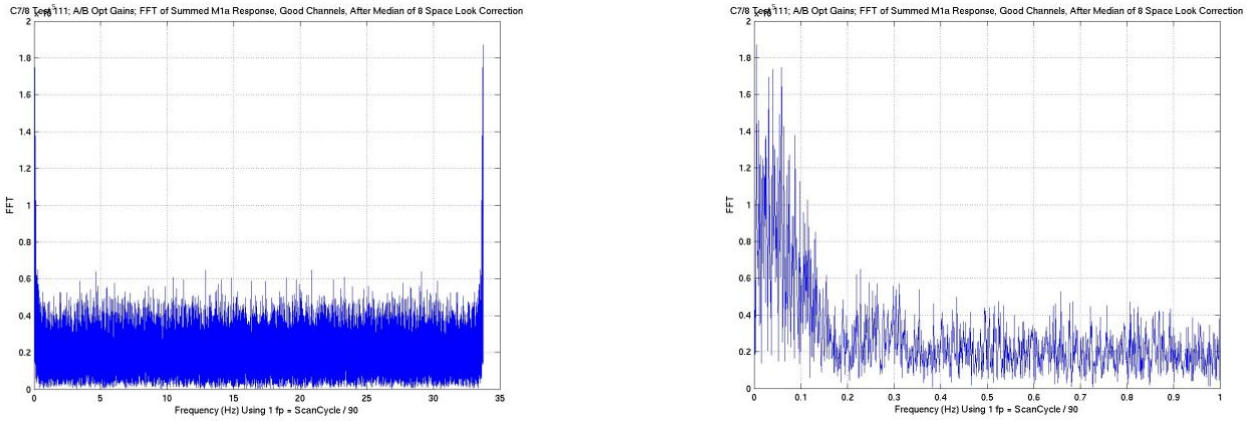

Figure 4. FFT of the sum of the data for all M1a channels in states 0-2 for Test 111, showing the full spectrum (left) and the low-frequency portion (right).

To check for possible inaccuracies due to the AIRS sampling, FFTs were performed on 39,400-point vectors of sinusoidal oscillations, both with full sampling and with simulated AIRS sampling, as a function of the frequency of the oscillation, and the resulting amplitudes and apparent frequencies were estimated from the position and amplitude of the maximum values of the FFTs. The results, in Figure 5, show very small effects on the apparent frequencies and up to 50% error in the apparent amplitude. These effects are significant but do not change the overall conclusion, that there is very little 1/f noise in the correlated AIRS noise (at least for Module M1a). This conclusion was checked by performing FFTs of all of the M1a data, removing the lowest-frequency points, then reversing the FFTs and re-calculating the covariance; the results were essentially the same.

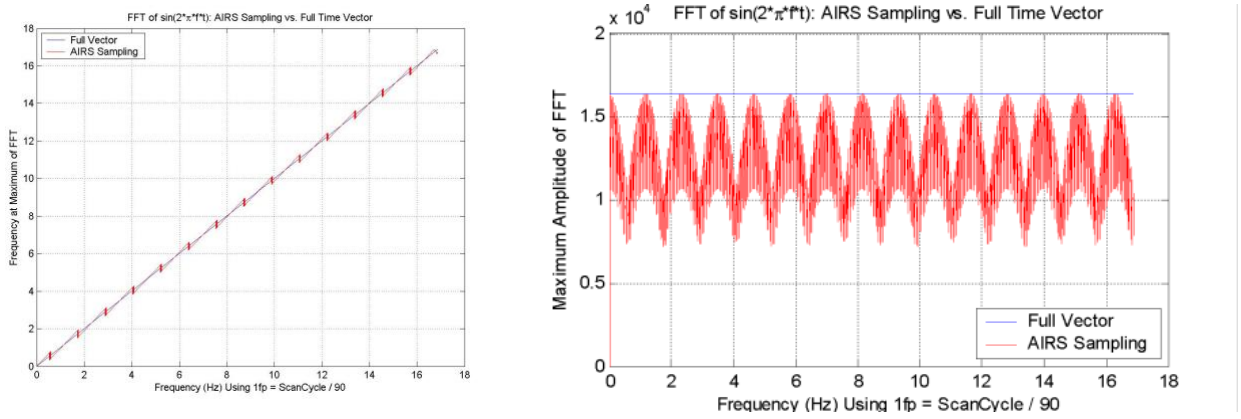

Figure 5. Comparison of apparent frequency (left) and amplitude (right) of FFTs of sinusoidal data, as a function of the frequency of the oscillation, for full sampling (blue) and simulated AIRS sampling of 90 points in every group of 119 (red). The effect of the AIRS sampling is to create sidebands, resulting in lower amplitudes and slight frequency shifts in the main peak.

V. DEPENDENCE ON A/B WEIGHT

The data presented so far represent primarily tests conducted with A/B Opt weights loaded for the PV modules. Figures 6 – 8 show histograms, for the PV detector modules, of the off-diagonal covariance values separated by weight pairings, i.e. A vs. A, B vs. B, and A vs. B compared to all channels in "good" states. For visibility, each histogram has been scaled by the total number of points in each distribution. The secondary peaks in the distributions for all good channels reflect the actual totals for the partial distributions, while the main or central peaks include additional pairings A=B vs. A=B, A=B vs. A, and A=B vs. B, occurring at values intermediate to the other pairings. Since the number of channels in states 1 and 2 increases with module number (going towards the longer wavelengths), the height of the secondary peaks also increases in this order.

Except for M3, which shows small and fairly uniform correlation for all pairings, there is a clear tendency for the A vs. B covariance to be smaller than A vs. A or B vs. B, and even negative (anti-correlation) for Modules M5 – M10, most strongly for M5. The A vs. A and B vs. B peaks are at different locations, but one is not systematically greater than the other, except for Modules M4c and M4d (Figure 7) , where the B vs. B peaks coincide with the A vs. B peaks.

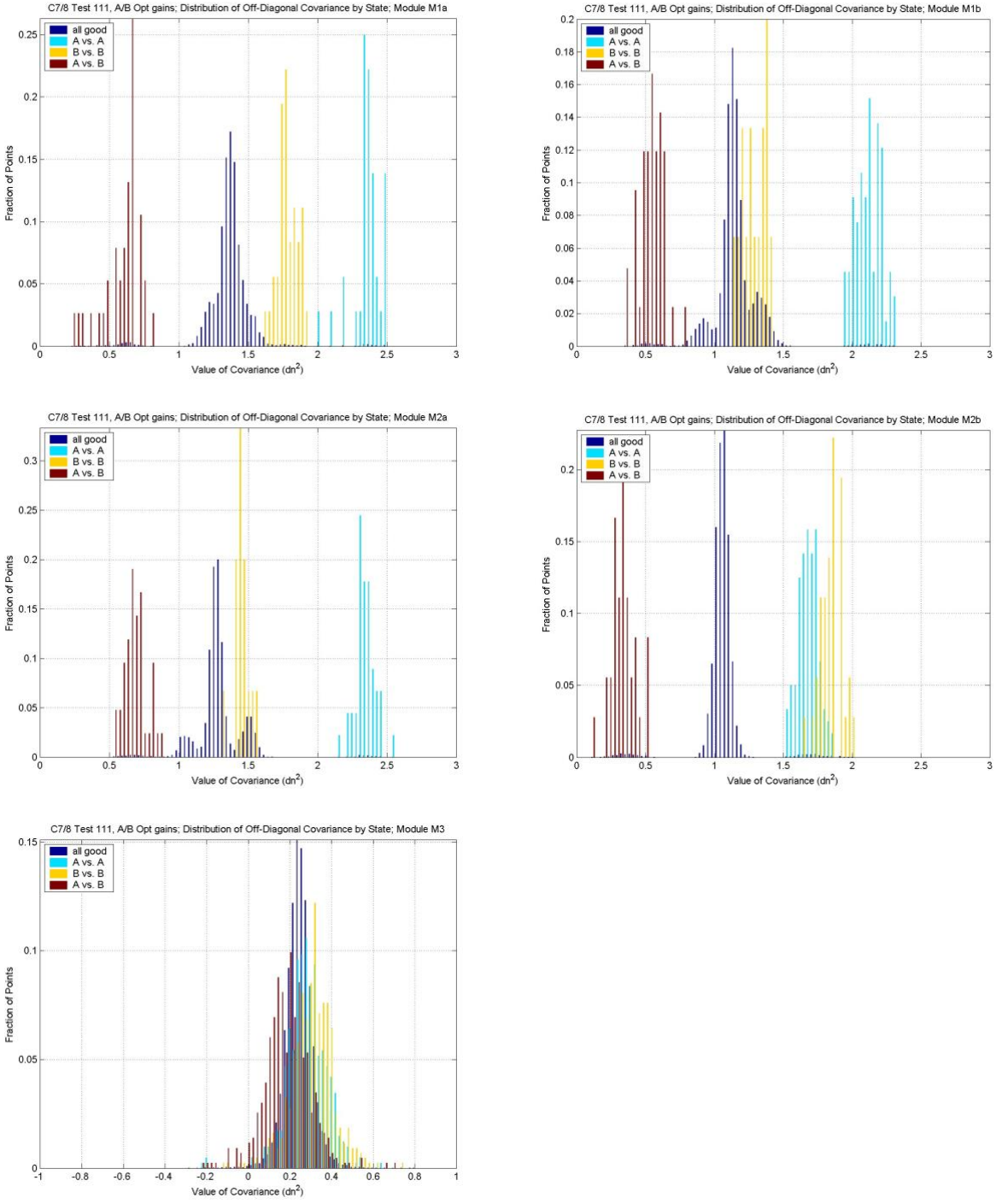

Figure 6. Distributions by A/B weight of the off-diagonal elements of the covariance matrix for Test 111, for the PV modules M1 – M3, for all "good" channels (blue, states 0-2), with only A weights (cyan, state 1), B weights (yellow, state 2) and A vs. B weights (magenta).

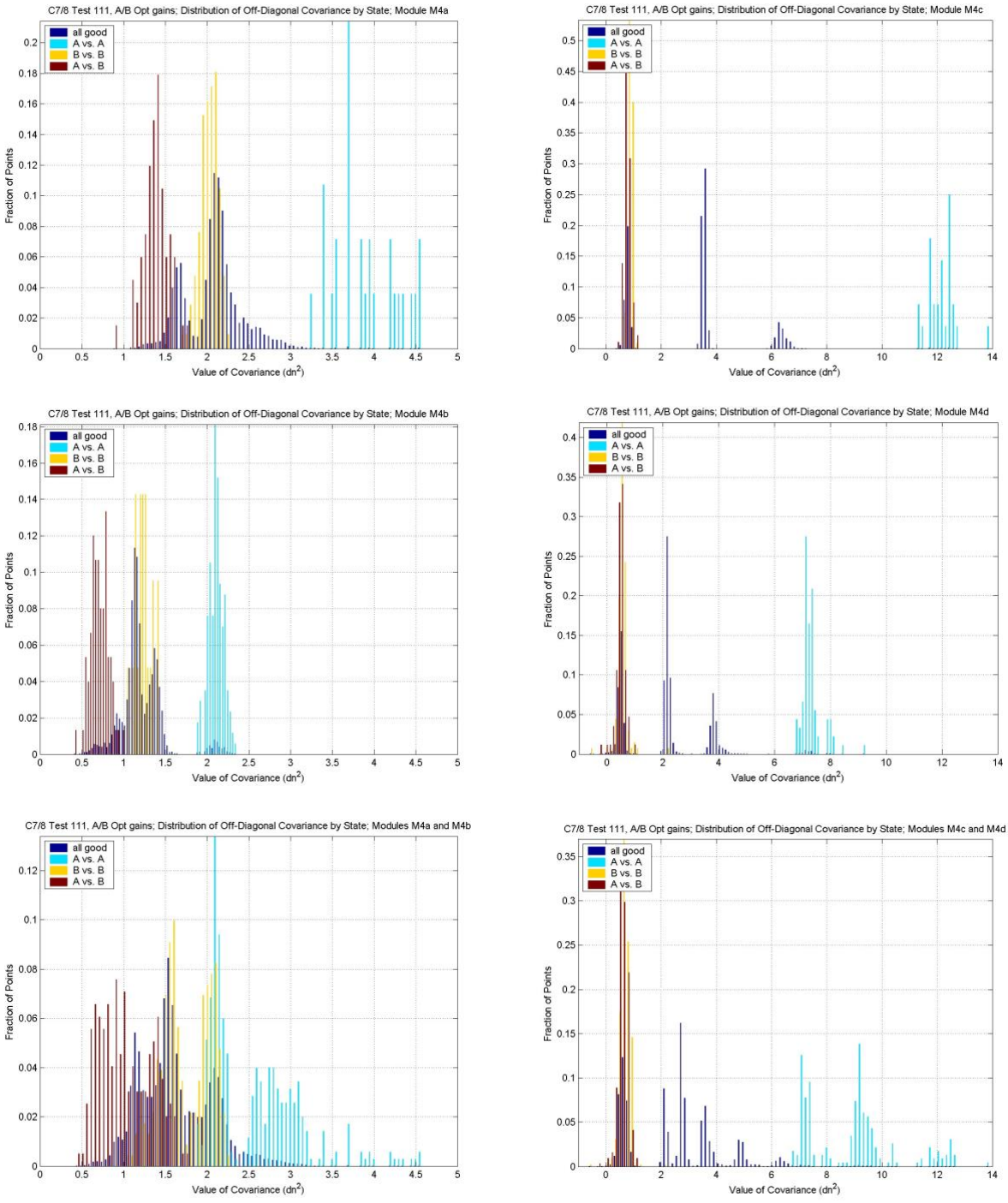

Figure 7. Same as Figure 6 but for Module 4, showing distributions within the separate detector modules M4a-d (upper 4 graphs) and within the common ROIC modules for the detector pairs M4a/M4b and M4c/M4d (lower 2 graphs).

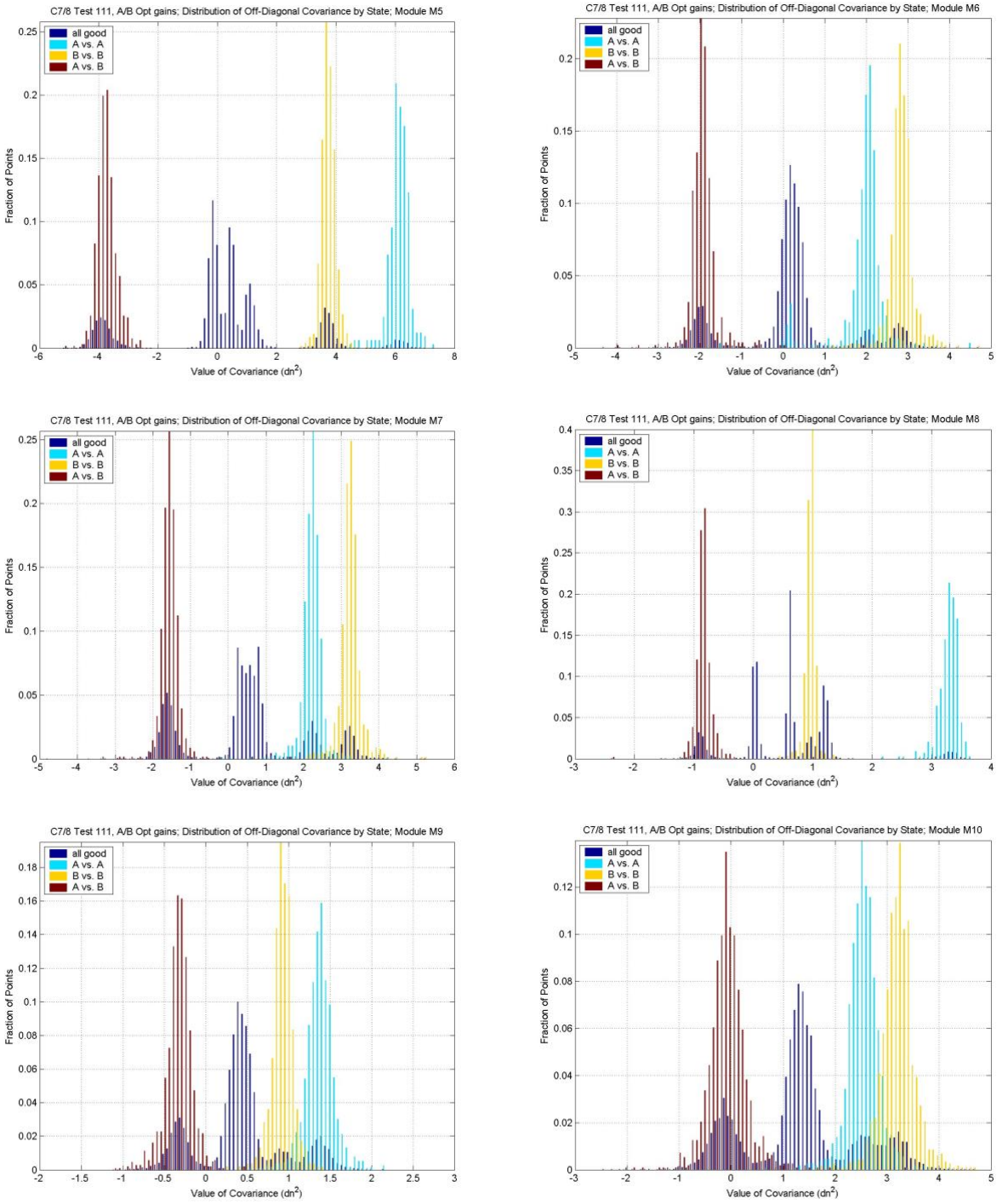

Figure 8. Same as Figures 6-7 but for Modules M5 – M10.

The case of M4 is very interesting for other reasons. In spite of the commonality of the ROICs, and even though Figure 1 shows a clear block of correlation across the internal detector boundaries, the histograms show clear differences between, for example, M4a and M4b, and a complex pattern for all good channels resulting from the different combinations of weight pairings. Extra peaks are seen, for example, for correlations between M4a and M4b channels.

A comparison of histograms by A/B state for Module 4c for Tests 94 and 111 gives additional details on the different correlation patterns seen in Figure 3 for these two tests. The distribution for Test 94, in Figure 9, shows peaks at the same locations as for Test 111, in the plot for M4c in Figure 7, but with a significant addition of peaks for A vs. B near covariance values of 6.5 dn^2 and a shift in the population of peaks for all good channels from values near 0.5, for Test 94, to values near 6.5 for Test 111, corresponding to the larger number of light bands in the right-hand plot in Figure 3.

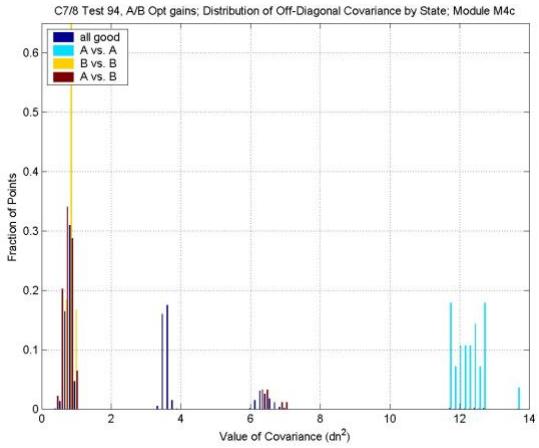

Figure 9. Same as Figures 6 – 9 but for Test 94, in a different FPA cool-down from Test 111, for module M4c.

VI. CORRELATIONS FOR NOISY CHANNELS

So far the data have been analyzed only for channels with well-behaved noise, i.e. where the A/B Opt selection process has eliminated most of the detectors with high or non-Gaussian noise and where the channels with remaining poor noise have been omitted from the plots. To investigate the effect for these noisy channels, the covariance matrix has been calculated for Test 103, with A weights, and the distributions compared for good- vs. poor-noise channels. The distributions were very broad for the poor-noise channels (in states 2 – 6 as determined in part from this test), too broad to be plotted on the

same graph as the distributions for good-noise channels. Instead, the distributions have been plotted in Figure 10, for a few representative modules, as "rank order" plots, where the vectors containing the covariance values are sorted then plotted in order. The y values of the flat portion of the plot corresponds to the x value of the peak of the histogram.

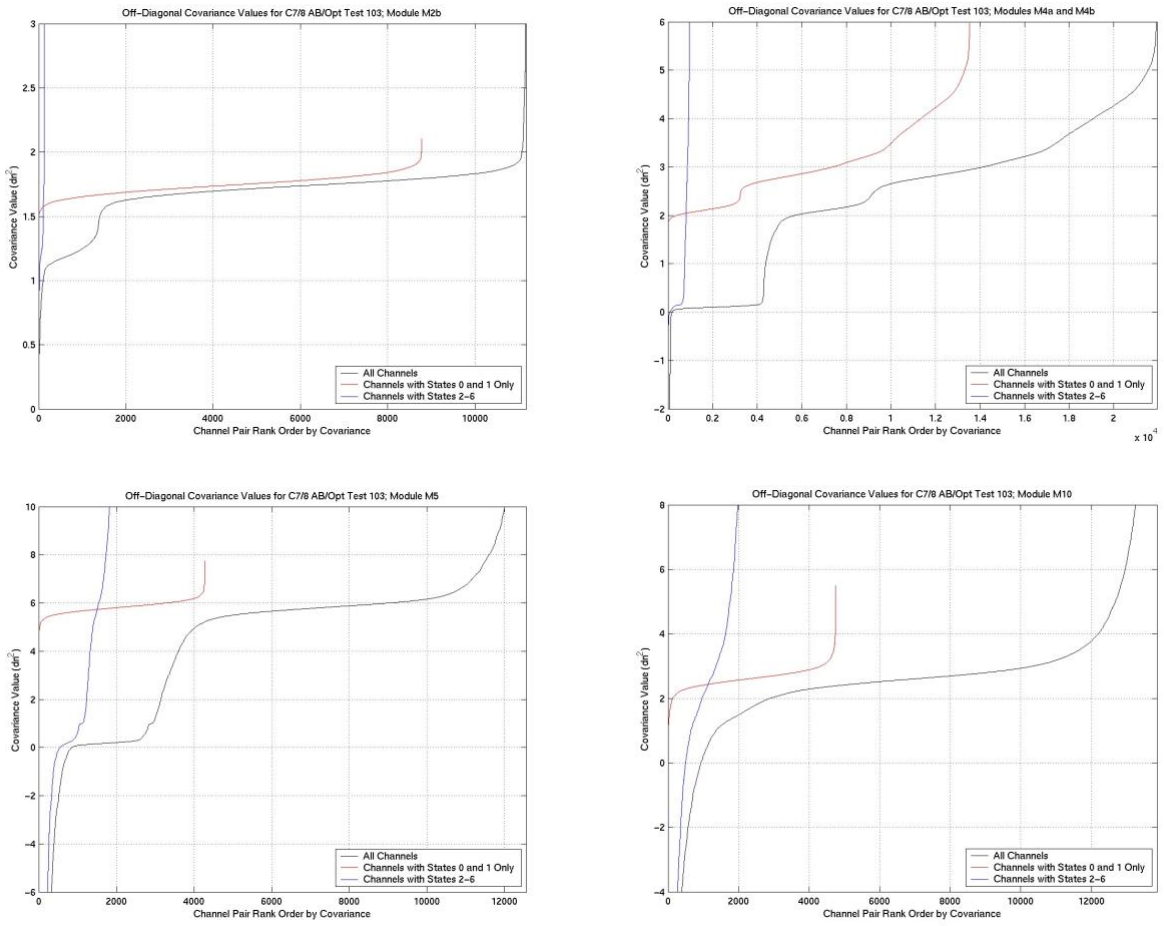

Figure 10. Rank order plots of the off-diagonal elements of the covariance matrix for Test 103, with A weights, for representative modules M2b, M4b, M5, and M10, showing data for all channels (black), only good-noise channels (red), and only poor-noise channels (blue).

The curves for the good-noise channels in Test 103 are in agreement with the distributions in Figure 6 – 8 for the A vs. A case, except for modules M6 and M7. Figure 11 shows, for these modules, plots for Test 103 and for Test 104, which used B weights; comparison of the curves shows that for these two

modules the curves for B vs. B represent higher values of covariance than the curves for A vs. A, as was the case for Test 111, but both curves are shifted to somewhat higher values compared to the respective Test 111 distributions in Figure 8.

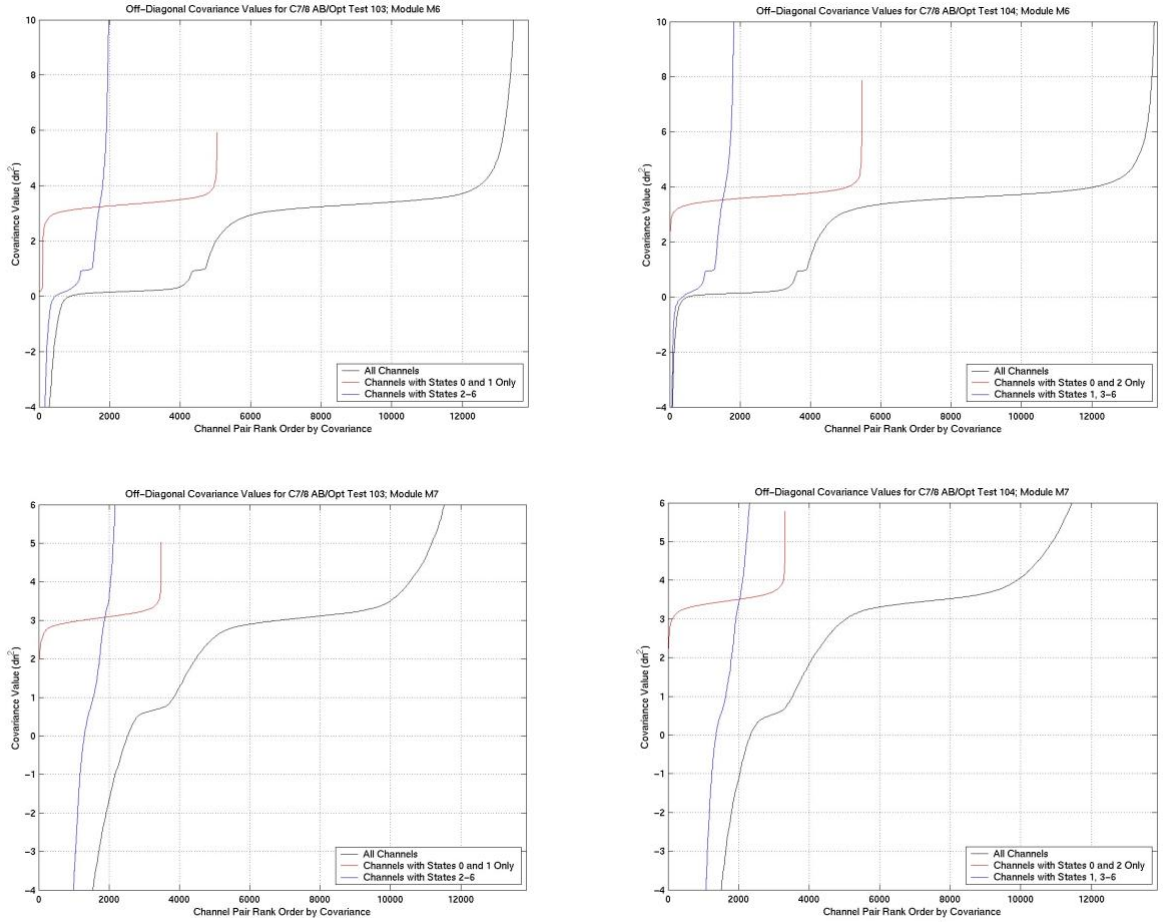

Figure 11. Same as Figure 10, for modules M6 and M7, but the right-hand plots are for Test 104,with B weights.

This completes the description of data supporting the summary points in Section I. Another topic of lesser interest is the subject of correlations from footprint to footprint within each AIRS scan cycle.

VII. WITHIN-SCAN CORRELATION

The same test data analyzed above for channel-to-channel correlations were also analyzed for correlations, for each channel, among the 90 AIRS scene footprints. The median-of-eight space look

correction is expected to introduce a correlation coefficient of approximately 1/8 since the space look noise power (effectively about 1/8 of the single-footprint noise because the median of 8 footprints is used) is added to the noise power of each of the footprints in a given scan. For each channel the 440x90 matrix of data points was analyzed to give a 90x90 covariance matrix. Figure 12 plots an estimate of the correlation coefficient as the ratio of the median of all off-diagonal values to the median of the diagonal values for each channel in states 0-2; the results are somewhat higher than the expected 1/8.

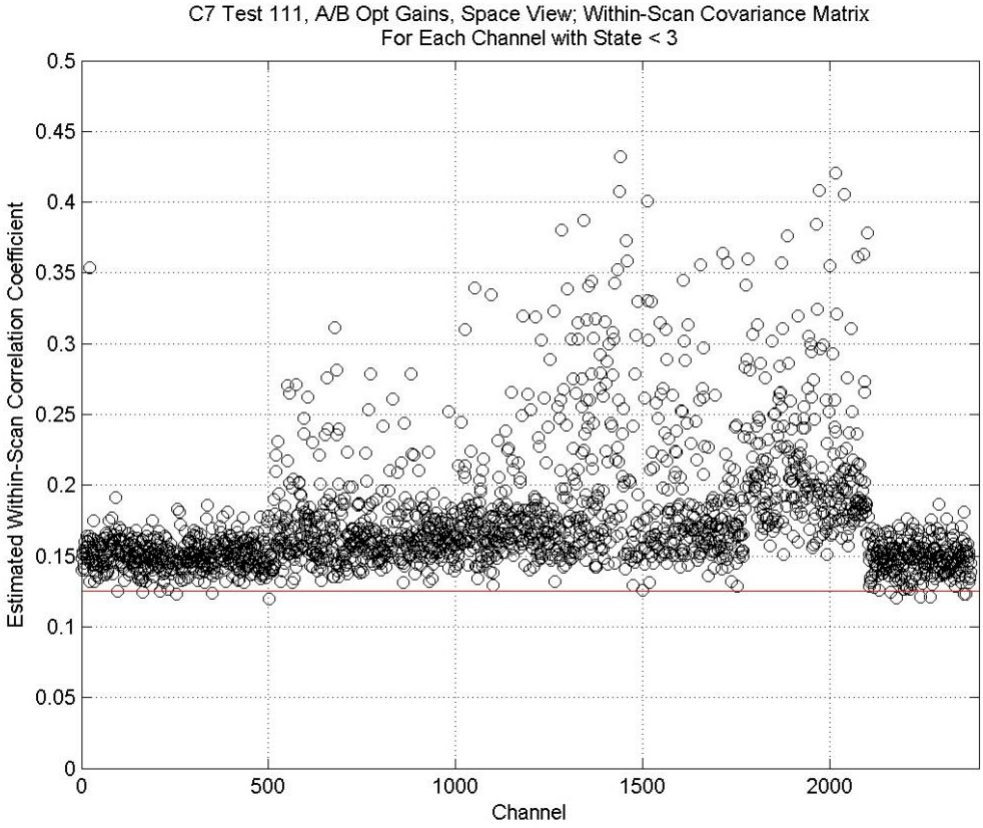

Figure 12. Estimated within-scan correlation coefficient for Test 111, compared to the expected value of 1/8 = 0.125.

Additional details of this correlation are given in Figures 13 and 14, where the data have been evaluated as a function of the distance between footprints then the median calculated for each module. The correlation for modules which do not exhibit drift (M1, M2, M11, and M12) also has no dependence on inter-footprint distance, whereas the other modules do exhibit a large dependence.

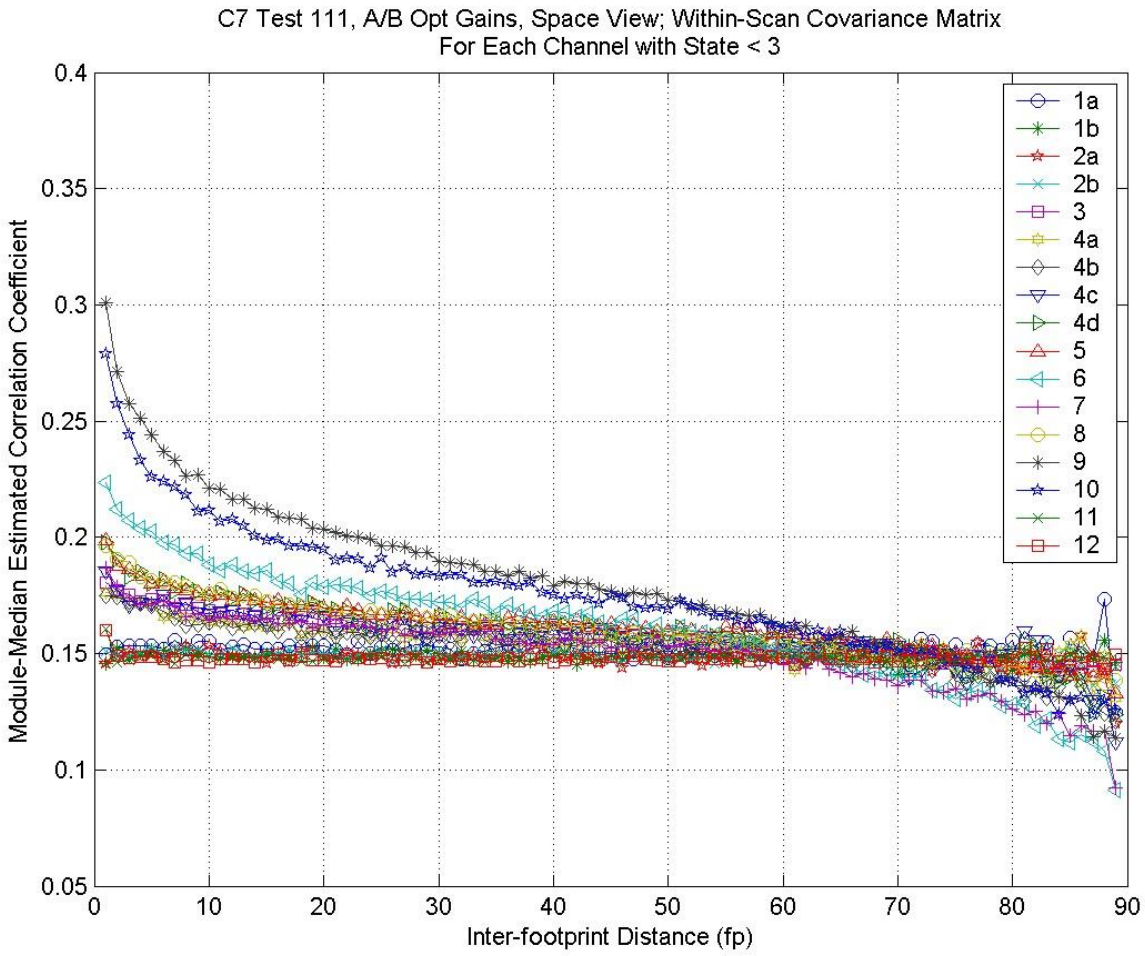

Figure 13. Estimated module-median correlation coefficients vs. distance between footprints.

VIII. DISCUSSION

The properties of the channel-to-channel correlated noise, listed in the Summary in Section I, point to the ROIC as the origin of this noise. The scene independence and lack of spectral cross-talk indicate some sort of noise source common to all of the channels within each affected group. Effects within the detector arrays are ruled out by the inter-detector-array correlation in module M4. Effects in the SEM electronics modules, which process the data output from the ROICs, are ruled out by the lack of correlation between modules. Details of the dependence on A/B weight may provide clues to the origin of this noise, as may comparisons with different module architectures of the different correlation levels for different modules, especially the low correlation in M3.

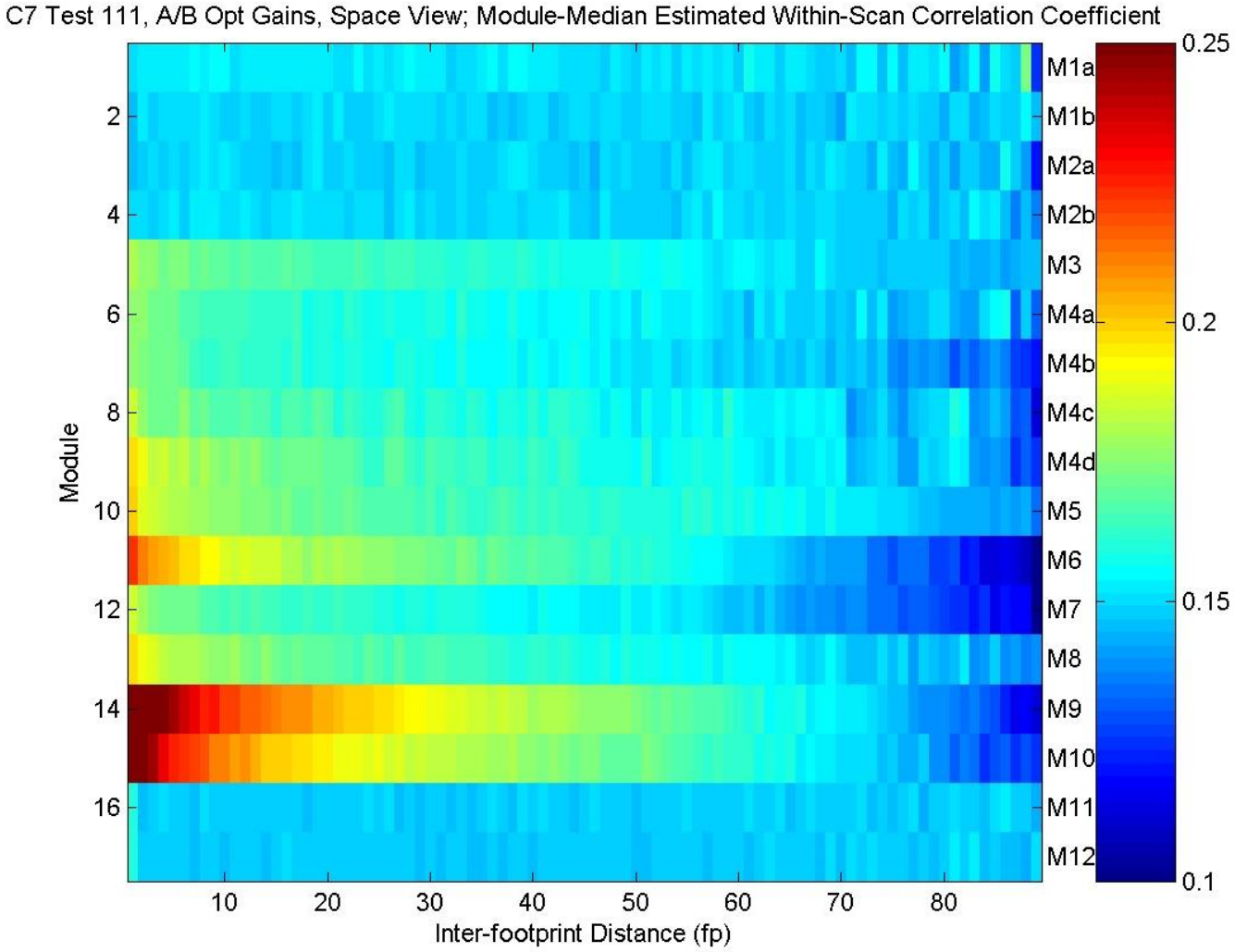

Figure 14. Image plot of the same data as in Figure 13.

[1] T. Pagano, "Estimation of AIRS Correlated Noise," ADF#614.
[2] M. Weiler, "AIRS-C2/C7: A/B Opt Gain Selection," ADF#602.
[3] M. Weiler, "AIRS-C7: Space View/OBC Noise Test," ADF#603.
[4] C. Barnet, "Status of L2 Retrieval System," AIRS Netmeeting on Detector Properties, Dec. 16, 2002.